Protein–Protein Interactions Hot Paper

DOI: 10.1002/ange.201404750

An Unusual Protein–Protein Interaction through Coupled Unfolding and Binding**

*Tae-Kyung Yu, Seung-A Shin, Eun-Hee Kim, Sunghyun Kim, Kyung-Seok Ryu, Haekap Cheong, Hee-Chul Ahn, Sangyong Jon, and Jeong-Yong Suh**

Abstract: *Aptides, a novel class of high-affinity peptides, recognize diverse molecular targets with high affinity and specificity. The solution structure of the aptide APT specifically bound to fibronectin extradomain B (EDB), which represents an unusual protein–protein interaction that involves coupled unfolding and binding, is reported. APT binding is accompanied by unfolding of the C-terminal β strand of EDB, thereby permitting APT to interact with the freshly exposed hydrophobic interior surfaces of EDB. The β-hairpin scaffold of APT drives the interaction by a β-strand displacement mechanism, such that an intramolecular β sheet is replaced by an intermolecular β sheet. The unfolding of EDB perturbs the tight domain association between EDB and FN8 of fibronectin, thus highlighting its potential use as a scaffold that switches between stretched and bent conformations.*

Fibronectin (FN), an essential component of the extracellular matrix, is a high-molecular-weight glycoprotein and exists as a disulfide-linked dimer comprised of two almost identical approximately 250 kDa subunits. FN interacts with collagen, heparin, and cell-surface receptors (such as integrin) to mediate wound healing, as well as cell adhesion, migration, and morphology.[1] The FN subunit comprises three types of repeating units: type I (40 aa), type II (60 aa), and type III (90 aa). The fibronectin extradomain B (EDB) is inserted between type III modules 7 and 8 (FN7 and FN8) by alternative splicing and its expression is linked to blood vessel formation during embryonic development and tumor vascularization.[2] EDB is expressed in the majority of aggressive solid human tumors but not in normal tissues or vessels; it is therefore a promising clinical biomarker for the detection and treatment of tumors.[3]

Aptides are a novel class of high-affinity peptides that can recognize diverse protein targets.[4a] In particular, an aptide specific for EDB (APT) has demonstrated its potential for use in cancer imaging and therapy.[4] To understand the structural determinants underlying the target specificity of aptides, we determined the complex structure of APT bound to EDB by using NMR spectroscopy. Unexpectedly, APT binding entails the unfolding of an entire C-terminal β strand of EDB, thereby exposing a wide hydrophobic surface (Figure 1). APT specifically interacts with the exposed surface of EDB and forms a tight complex. The interaction between APT and EDB thus demonstrates an unusual example of protein complex formation by coupled unfolding and binding. The unfolding-and-binding mechanism is reversible: dissociation of APT restores the fold of intact EDB. Herein, we address the structural and energetic details of coupled unfolding and binding and discuss its potential applications.

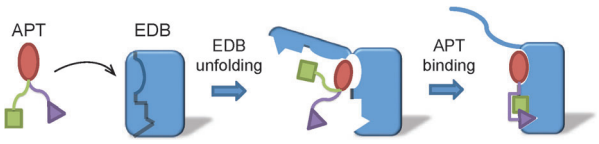

Figure 1. A schematic illustration of coupled unfolding and binding in the interaction between APT and EDB. The β hairpin of APT is shown as a red oval and the target-binding arms are shown as a green square and a purple triangle. The C-terminal β strand of EDB opens and unfolds and APT specifically interacts with the exposed hydrophobic surfaces.

The EDB:APT complex is in slow exchange on the chemical shift time scale and has a 1:1 binding stoichiometry. The backbone amide resonances of EDB show extensive chemical shift perturbations upon binding to APT, thus implying a large conformational change upon complex formation (Figure S1 in the Supporting Information). In particular, residues in β strands F and G as well as in loop C′E of EDB exhibited significant chemical shift perturbations. We carried out a suite of three-dimensional heteronuclear correlation NMR experiments to obtain backbone and side-chain assignments of the EDB:APT complex. The complex structure was determined by using 1907 NMR restraints, including 1610 experimental NOE restraints, 225 dihedral-

[*] T. K. Yu, S. A. Shin, Prof. Dr. J. Y. Suh
Biomodulation Major, Department of Agricultural Biotechnology
Seoul National University, 1 Gwanak-ro, Gwanak-gu
Seoul 151-921 (South Korea)
E-mail: jysuh@snu.ac.kr
E. H. Kim, Dr. K. S. Ryu, Dr. H. Cheong
Division of Magnetic Resonance, Korea Basic Science Institute
16 Yeongudanji-Ro, Ochang, Chungbuk 363-883 (South Korea)
Dr. S. Kim, Prof. Dr. S. Jon
KAIST Institute for the BioCentury, Department of Biological Sciences, Korea Advanced Institute of Science and Technology
291 Daehak-ro, Daejeon 305-701 (South Korea)
Prof. Dr. H. C. Ahn
Department of Pharmacy, Dongguk University-Seoul
Dongguk-ro 32, Ilsandong-gu, Goyang
Gyeonggi, 410-820 (South Korea)

[**] This work was supported by a National Research Foundation of Korea (NRF) grant (2013R1A1A2010856). We thank the high-field NMR facility at the Korea Basic Science Institute and the National Center for Inter-University Research Facilities.

Supporting information for this article is available on the WWW under http://dx.doi.org/10.1002/anie.201404750.

angle restraints, 72 backbone $^{1}D_{NH}$ residual dipolar couplings, and 29 hydrogen-bonding restraints. Structures were calculated by simulated annealing using the Xplor-NIH program.[5] A summary of the structural statistics of the EDB:APT complex is provided in Table S1 in the Supporting Information.

Free EDB comprises seven β strands that form a β sandwich structure, which is well conserved between fibronectin type III repeats.[6] The solution structure of free EDB was previously determined by NMR spectroscopy, with three stands (A, B, and E) forming one β sheet and four strands (C, C′, F, and G) forming another β sheet (Figure 2a).[7] EDB in

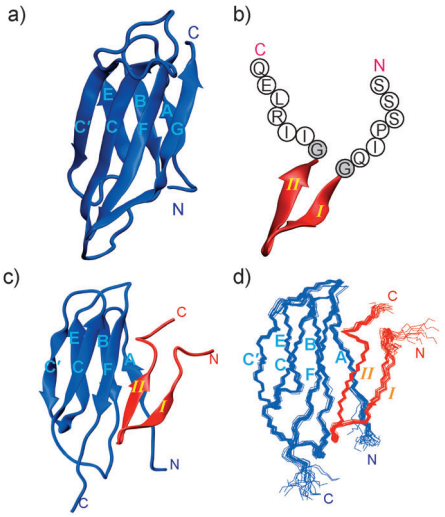

Figure 2. The solution structures of EDB and APT in their free and complexed states. a) Free EDB (residues 8–95) with seven β strands (βA–βG) shown as a ribbon diagram (PDB code 2fnb). b) Free APT with the β hairpin (PDB code 1Le0) shown as a ribbon diagram and the amino acid sequence given for the flanking target-binding arms. The two glycine linker residues are shaded in gray. c) The complex structure of EDB (blue) and APT (red) shown as a ribbon diagram (PDB code 2mnu). d) The superposition of 20 energy-minimized conformers of the EDB:APT complex. In the complex structure, the disordered βG of EDB (residues 86–95) is omitted for clarity.

the complex maintains a similar β-sandwich fold by six β strands (Figure 2c). Surprisingly, the C-terminal β strand completely unfolds in the complex and is replaced by β strand *II* of APT. Superposition of the backbone atoms for the ensemble of the final 20 simulated annealing structures demonstrates that the six β strands of EDB are well ordered to maintain the β sandwich structure and associate with APT to form an intermolecular antiparallel β sheet (Figure 2d). APT is comprised of a central β-hairpin structure and flanking target-binding arms of six variable residues (Figure 2b).[4a,8] The target-binding arms adopt a well-defined conformation in which the C-terminal arm is in closer contact with EDB (Figure 2c and d). The two arms are bent at *Arg223* (C-terminus) and *Pro204* (N-terminus), such that they extend in a tweezer-like conformation. The heteronuclear ^{1}H-^{15}N NOE data confirm that the target-binding arms are highly ordered except for at the N-terminus (Figure S2).

The unfolding of β strand G of EDB upon binding to APT is supported by several lines of experimental evidences. First, a comparison of heteronuclear ^{1}H-^{15}N NOE data between free EDB and the EDB:APT complex reveals a marked difference in the β-strand G region (Figure 3). Large NOE

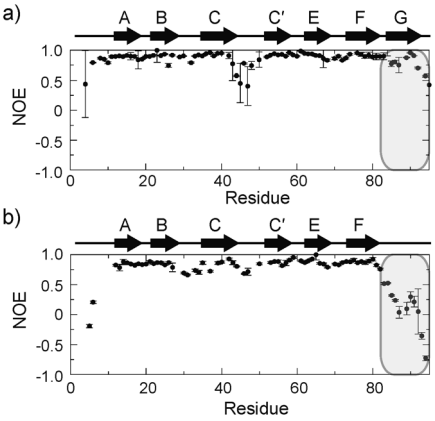

Figure 3. ^{1}H-^{15}N heteronuclear NOE data as a function of the residue number of EDB in the free state (a) and in complex with APT (b). NOE data from β strand G are highlighted by shaded boxes.

values (>0.8) were observed in β strand G of free EDB as well as the other six β strands. EDB in the complex, however, showed significantly reduced NOE values (<0.4) in the β-strand G region (residues 84–93), thus clearly indicating that β strand G becomes disordered upon binding. Second, the $EDB_{5–83}$ mutant (residues 5–83), which was truncated at the C-terminus to remove β strand G, showed a remarkably similar ^{1}H-^{15}N HSQC spectrum to that of wild-type EDB when in complex with APT (Figure S3). With the exception of missing resonances from the truncation, the backbone amide chemical shifts were mostly identical. We also monitored HSQC spectra of ^{15}N-APT in complex with EDB or $EDB_{5–83}$. Again, the backbone chemical shifts of APT were indistinguishable between the two complexes (Figure S4). The chemical shift perturbation profiles confirm that β strand G remains disordered in the complex and does not interact with APT. Third, the ^{15}N R_2 relaxation rates of the backbone amides in β strand G were greatly reduced in the complex, an effect that is typically observed in disordered tail regions.

The binding interface is an elongated ellipsoid primarily formed by β strands A and F of EDB, and β strand *II* and the target-binding arms of APT (Figure 4a). The interaction interface is relatively flat and buries approximately 670 Å^2 of EDB and 840 Å^2 of APT. The interaction interface of EDB comprises Leu12, Phe14, Ile17 (β strand A); Asp19 (loop AB); Ile22 (β strand B); Glu68 (loop EF); and Asp72–Thr79 (β strand F). The interaction interface of APT comprises *Pro204* and *Ile205* (N-terminal arm), *Trp209* (β strand *I*), *Trp216–Lys219* (β strand *II*), *Ile222–Leu224* (C-terminal arm; Figure 4b). Overall, the interaction interface features a hydrogen-bonding network between backbone amide groups to form an intermolecular β sheet, which is further stabilized by hydrophobic and electrostatic interactions between side-

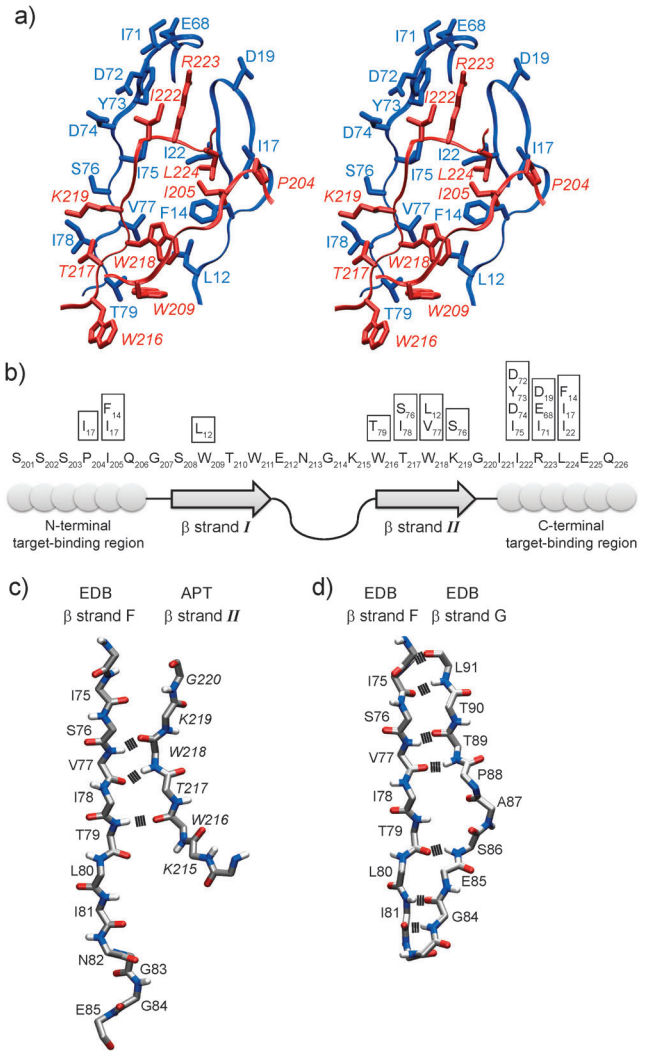

Figure 4. The interface between EDB and APT. a) The interfacial residues of EDB are shown in in blue and APT is shown in red, with the backbone shown as a tube and the side chains shown as sticks models. b) A diagrammatic representation of the intermolecular contacts between EDB and APT. The residues of EDB in contact with APT are shown in boxes above the interfacial residues of APT. c) The intermolecular hydrogen bonds between β strand F of EDB and β strand *II* of APT in the complex. d) The intramolecular hydrogen bonds between β strands F and G in free EDB. The hydrogen bonds between the β strands are indicated by black squares.

chain groups. Intermolecular hydrogen bonds are formed between the backbone amide groups of β strand F of EDB and β strand *II* of APT. Specifically, Thr79 forms a hydrogen bond with *Trp216*, and Val77 forms a pair of hydrogen bonds with *Trp218* (Figure 4c). In free EDB, the amide group of Thr79 does not participate in the hydrogen bond because Ala87 in the opposite strand protrudes to form a β-bulge structure (Figure 4d). Val77 forms hydrogen bonds with Thr89 in free EDB and is replaced by *Trp218* of APT in the complex. Our structure of the EDB:APT complex is consistent with previous finding that the C-terminal target-binding arm is more important for the binding affinity than the N-terminal arm.[4a]

EDB is a highly acidic protein (theoretical isoelectric point (p*I*) = 3.6), the electrostatic surface potential of which shows a wide distribution of negative charges (Figure S5). The unfolding of β strand G exposes a wide hydrophobic interior region that provides the key interaction surface for APT. For example, the hydrophobic patch formed by Phe14, Ile17, and Ile22 of EDB is exposed by unfolding and provides the interface for *Pro204*, *Ile205*, and *Leu224* of APT (Figure 4a and Figure S5). Similarly, Leu12 and Val77 are exposed to provide the interface for *Trp209* and *Trp218*. In addition, Asp72–Ile75 in β strand F of EDB participate in van der Waals interactions with *Ile222*. Finally, Asp19, Glu68, and Ile71 are in close contact with *Arg223* through electrostatic and hydrogen-bonding interactions. The key residues in the target-binding arms of APT are thus *Ile222*, *Arg223*, and *Leu224* of the C-terminal arm, and *Pro204* and *Ile205* of the N-terminal arm.

To understand the energetics of coupled unfolding and binding, we explored the binding thermodynamics of EDB and APT by using a series of C-terminal truncation mutants of EDB (Table 1). The ^{1}H-^{15}N HSQC spectra of individual EDB mutants in complex with APT indicated that the complex structures were essentially the same, differing only in the

Table 1: Thermodynamic parameters for the interaction between EDB (or EDB mutants) and APT, and between EDB–FN8 and APT. Equilibrium dissociation constants (K_D), binding free energy (ΔG), binding enthalpy (ΔH), and binding entropy (ΔS) values were obtained from isothermal titration calorimetry at 25 °C.

	K_D [nM]	ΔG [kcal mol^{-1}]	ΔH [kcal mol^{-1}]	$-T\Delta S$ [kcal mol^{-1}]
EDB	230 ± 36	−9.0 ± 0.1	2.8 ± 0.0	−11.8 ± 0.1
EDB_{5-94}	170 ± 33	−9.2 ± 0.1	−2.1 ± 0.0	−7.1 ± 0.1
EDB_{5-92}	100 ± 40	−9.6 ± 0.2	−3.8 ± 0.1	−5.8 ± 0.2
EDB_{5-90}	91 ± 24	−9.6 ± 0.2	−4.4 ± 0.1	−5.2 ± 0.2
EDB_{5-86}	110 ± 37	−9.5 ± 0.2	−4.7 ± 0.1	−4.8 ± 0.2
EDB_{5-83}	120 ± 32	−9.5 ± 0.2	−4.6 ± 0.1	−4.9 ± 0.2
EDB-FN8	3200 ± 300	−7.5 ± 0.1	6.6 ± 0.1	−14.1 ± 0.1

lengths of the unfolded C-terminal tail region. The thermodynamic profile of complex formation, however, was markedly changed by the truncation. Complex formation between EDB and APT is predominantly driven by a large entropic gain ($-T\Delta S = -11.8$ kcal mol^{-1}), which was consistent with the observed β strand G unfolding (Table 1). The enthalpic change ($\Delta H = 2.8$ kcal mol^{-1}) was slightly unfavorable, which is attributed to the energetic cost of unfolding β strand G. C-terminal truncations reduced both the entropic gain and the enthalpic cost of unfolding. Notably, the deletion of a single C-terminal residue dramatically changed the ΔH and $-T\Delta S$ profiles, whereas further truncations resulted in smaller changes. This observation indicates that β strand G is less stable at the N-terminus than at the C-terminus. We suppose that the β bulge of β strand G likely destabilizes the intramolecular hydrogen-bonding network (Figure 4d). In contrast to the ΔH and $-T\Delta S$ profiles, ΔG was only modestly changed by the truncation. The complete removal of β strand G in EDB_{5-83} resulted in large favorable enthalpic change

($\Delta H = -4.6\ \mathrm{kcal\,mol^{-1}}$), but also much reduced entropic contribution ($-T\Delta S = -4.9\ \mathrm{kcal\,mol^{-1}}$) for APT binding compared to intact EDB. As a consequence, the equilibrium dissociation constant (K_D) for EDB_{5-83}:APT indicated only a two-fold higher affinity than that of EDB:APT. A comparison of binding thermodynamics between EDB and EDB_{5-83} separates the ΔG values of the unfolding and binding events, thereby revealing that the overall ΔG value for coupled unfolding and binding is mainly determined by the ΔG value for binding and not the ΔG value for unfolding.

It is notable that an isolated β-hairpin scaffold of APT (*Ser208–Lys219*) could bind to EDB in a similar manner. The β-hairpin scaffold caused significant line-broadening for EDB, which mainly affects residues with large chemical-shift perturbations on APT binding. The line broadening indicates that the β-hairpin scaffold binds to EDB but easily dissociates owing to the absence of stabilizing target-binding arms. We propose that the coupled unfolding of EDB and binding of APT proceeds in two steps. First, the β-hairpin scaffold binds to the hydrophobic interior surface of EDB that is exposed by unfolding, thereby forming a weak transient complex. Second, the target-binding arms provide favorable interactions to form a stable complex.

In cellular fibronectin, individual FN domains are tightly associated through their loop regions to form an extended rod-like structure.[5] The interdomain interfaces between FN subunits determine domain orientation and loop structures, which are important for the molecular interactions and biological functions of FN.[9] For example, the insertion of EDB between FN7 and FN8 alters the domain orientation and interface of FN8, which promotes cell adhesion and spreading.[10] Since APT unfolds the C-terminal β strand of EDB, APT binding could affect the domain association between EDB and FN8. The ^{1}H-^{15}N HSQC spectrum of covalently linked ^{15}N-EDB–FN8 showed noticeable chemical shift changes from the overlaid HSQC spectra of separately expressed domains (Figure S6). The chemical-shift perturbation in the loop regions indicates that the two domains associated through their loop regions as expected. The HSQC spectrum of the ^{15}N-EDB–FN8:APT complex, on the other hand, was remarkably similar to the superimposed spectra of individual ^{15}N-EDB:APT and ^{15}N-FN8:APT complexes, thus indicating that EDB in complex with APT was no longer associated with FN8. The binding affinity between EDB–FN8 and APT was reduced by 14-fold compared to that between EDB and APT, with the K_D value measured as 3.2 μM (Table 1). The reduced binding was caused by a large increase in unfavorable enthalpic contributions, a result that can be explained by the extra energetic cost to break the loop interactions between EDB and FN8. Taken together, our results demonstrate that the binding of APT to EDB–FN8 and the unfolding of β strand G perturb the domain association of EDB and FN8, thereby disengaging the two domains from each other. Perturbation of the domain interaction between EDB and FN8 may change the global FN structure and loop conformations, thereby altering EDB-associated angiogenic signaling. In addition, interconversion of the EDB–FN8 structure between a rigid elongated form and a flexible form could be implemented as a molecular scaffold that switches between stretched and bent conformations on APT binding, thereby altering its tensile and bend strengths.

The coupled unfolding and binding of EDB and APT demonstrates that protein–protein interactions can generate a specific binding interface through unfolding. The unfolding-and-binding mechanism has several biological implications. First, it expands the diversity of known protein–protein interactions. Unfolding and binding allows for interaction through buried interfaces, so that variations in hydrophobic interior residues as well as surface-exposed residues can contribute to the binding specificity. Second, the stability of the secondary structure that unfolds may modulate the binding affinity. Since unfolding of the secondary structure is balanced by an enthalpic cost and an entropic gain, the folding propensity of the secondary structure can offer a new option for modulating the binding affinity. Finally, characterizing the structural determinants that dictate protein unfolding and binding may help in the prediction and design of inhibitors that target protein–protein interactions.

Received: April 28, 2014
Published online: July 1, 2014

Keywords: aptides · fibronectin · NMR spectroscopy · protein folding · protein–protein interactions

[1] R. Pankov, K. M. Yamada, *J. Cell Sci.* **2002**, *115*, 3861 – 3863.
[2] a) A. R. Kornblihtt, K. Vibe-Pedersen, F. E. Baralle, *Nucleic Acids Res.* **1984**, *12*, 5853 – 5868; b) G. Nicolò, S. Salvi, G. Oliveri, L. Borsi, P. Castellani, L. Zardi, *Cell Differ. Dev.* **1990**, *32*, 401 – 408.
[3] a) L. Zardi, B. Carnemolla, A. Siri, T. E. Petersen, G. Paolella, G. Sebastio, F. E. Baralle, L. Zardi, *EMBO J.* **1987**, *6*, 2337 – 2342; b) M. Kaspar, L. Zardi, D. Neri, *Int. J. Cancer* **2006**, *118*, 1331 – 1339.
[4] a) S. Kim, S. D. Kim, H. H. Jung, I. H. Lee, J. I. Kim, J. Y. Suh, S. Jon, *Angew. Chem.* **2012**, *124*, 1926 – 1930; *Angew. Chem. Int. Ed.* **2012**, *51*, 1890 – 1894; b) J. Park, S. Kim, P. E. Saw, I. H. Lee, M. K. Yu, M. Kim, K. Lee, Y. C. Kim, Y. Y. Jeong, S. Jon, *J. Controlled Release* **2012**, *163*, 111 – 118; c) H. Kim, Y. Lee, I. H. Lee, S. Kim, D. Kim, P. E. Saw, J. Lee, M. Choi, Y. C. Kim, S. Jon, *J. Controlled Release* **2014**, *178*, 118 – 124; d) P. E. Saw, S. Kim, I. H. Lee, J. Park, M. Yu, J. Lee, J. I. Kim, S. Jon, *J. Mater. Chem. B* **2013**, *1*, 4723 – 4726.
[5] C. D. Schwieters, J. Kuszewski, G. M. Clore, *Prog. Nucl. Magn. Reson. Spectrosc.* **2006**, *48*, 47 – 62.
[6] D. J. Leahy, I. Aukhil, H. P. Erickson, *Cell* **1996**, *84*, 155 – 164.
[7] R. Fattorusso, M. Pellecchia, F. Viti, P. Neri, D. Neri, K. Wüthrich, *Structure* **1999**, *7*, 381 – 390.
[8] A. G. Cochran, N. J. Skelton, M. A. Starovasnik, *Proc. Natl. Acad. Sci. USA* **2001**, *98*, 5578 – 5583.
[9] a) S. Bencharit, C. B. Cui, A. Siddiqui, E. L. Howard-Williams, J. Sondek, K. Zuobi-Hasona, I. Aukhil, *J. Mol. Biol.* **2007**, *367*, 303 – 309; b) A. Schiefner, M. Gebauer, A. Skerra, *J. Biol. Chem.* **2012**, *287*, 17578 – 17588.
[10] M. Hashimoto-Uoshima, Y. Z. Yan, G. Schneider, I. Aukhil, *J. Cell Sci.* **1997**, *110*, 2271 – 2280.

